magmas originated in relatively warm basaltic crust at lower pressures than at present[3]. Simple scaling shows that, at the same potential mantle temperature, the subducting oceanic crust would have been a few hundred degrees warmer if the Archaean plate scale was of the order of the upper-mantle thickness. A low potential temperature of the early to mid-Archaean upper mantle is consistent with the results of thermobarometry[25]. MgO-rich Archaean komatiites[3,26] may have originated in the relatively hot boundary layer between the mantle layers. This boundary layer is significantly cooler or even non-existent after the transition, thereby explaining the absence of these komatiites in the post-Archaean. The increase in the volume of the sediments and the decrease in atmospheric temperature at the transition may be related to the growth of the continents: an increase in continental surface area increases the weathering rate and the rate of removal of the greenhouse-gas CO_2 from the atmosphere[27]. The formation of the shelves may indicate a dramatic drop in continental freeboard which may, at least partly, be attributed to a substantial increase in ocean water mass through increased degassing of the mantle. □

Received 23 February; accepted 7 November 1995.

1. Armstrong, R. L. *Austr. J. Earth Sci.* **38,** 613–630 (1991).
2. Taylor, S. R. & McLennan, S. M. *The Continental Crust: its Composition and Evolution* (Blackwell Scientific, Boston, 1985).
3. Taylor, S. R. & McLennan, S. M. *Rev. Geophys.* **33,** 241–265 (1995).
4. Kröner, A. *Precambrian Plate Tectonics* (Elsevier, Amsterdam, 1981).
5. Condie, K. C. *Archaean Crustal Evolution* (Elsevier, Amsterdam, 1984).
6. Percival, J. A. in *Archean Crustal Evolution* (ed. Condie, K. C.) 357–410 (Elsevier, Amsterdam, 1994).
7. Kasting, J. F. *Science* **259,** 920–926 (1993).
8. Des Marais, D. J. in *Archean Crustal Evolution* (ed. Condie, K. C.) 505–523 (Elsevier, Amsterdam, 1994).
9. Crowley, T. J. *Rev. Geophys. Space Phys.* **21,** 828–877 (1983).
10. Hale, C. J. *Nature* **329,** 233–237 (1986).
11. Christensen, U. & Yuen, D. A. *J. geophys. Res.* **90,** 10291–10300 (1985).
12. Tackley, P. J. *Rev. Geophys.* **33** Suppl., 275–282 (1995).
13. Steinbach, V., Yuen, D. A. & Zhao, W. *Geophys. Res. Lett.* **20,** 1119–1122 (1993).
14. Yuen, D. A. *et al. Phys. Earth planet Inter.* **86,** 185–203 (1994).
15. Solheim, L. P. & Peltier, W. R. *J. geophys. Res.* **99,** 6997–7018 (1994).
16. Stein, M. & Hofman, A. W. *Nature* **372,** 63–68 (1994).
17. Calvert, A. J., Sawyer, E. W., Davis, W. J. & Ludden, J. N. *Nature* **375,** 670–674 (1995).
18. Spohn, T. & Schubert, G. *J. geophys. Res.* **87,** 4682–4696 (1982).
19. Spohn, T. & Breuer, D. in *Evolution of the Earth and Planets* (eds Takahashi, E., Jeanloz, R. & Rubie, D. C.) 55–71 (Geophys. Monogr. Ser. 74, Am. Geophys. Union, Washington DC, 1993).
20. Stevenson, D. J., Spohn, T. & Schubert, G. *Icarus* **54,** 466–489 (1983).
21. Schubert, G. & Reymer, A. P. S. *Nature* **316,** 336–339 (1985).
22. Galer, S. J. G. *Earth planet. Sci. Lett.* **105,** 214–228 (1993).
23. McGovern P. & Schubert, G. *Earth planet. Sci. Lett.* **96,** 27–37 (1989).
24. Armstrong, R. L. *Phil. Trans. R. Soc. Lond.* A **301,** 433–471 (1981).
25. Boyd, F. P. & Gurney, J. J. *Science* **232,** 427–477 (1986).
26. Arndt, N. T. in *Archean Crustal Evolution* (ed. Condie, K. C.) 11–44 (Elsevier, Amsterdam, 1994).
27. Tajika, E. & Matsui, T. in *Origin of the Earth* (eds Newsom, H. E. & Jones, J. H.) 347–370 (Oxford Univ. Press, 1990).

ACKNOWLEDGEMENTS. This work was supported by the Deutsche Forschungsgemeinshaft.

Unexpected dominance of high frequencies in chaotic nonlinear population models

Joel E. Cohen

Rockefeller University, 1230 York Avenue, New York, New York 10021-6399, USA; and NERC Centre for Population Biology, Imperial College, Silwood Park, Ascot SL5 7PY, UK

BECAUSE water has a higher heat capacity than air, large bodies of water fluctuate in temperature more slowly than does the atmosphere[1]. Marine temperature time series are 'redder' than atmospheric temperature time series by analogy to light: in red light, low-frequency variability has greater amplitude than high-frequency variability, whereas in white light all frequencies have the same amplitude[2]. Differences in the relative importance of high- and low-frequency variability in different habitats affect the population dynamics of individual species and the structure of ecological communities[3–9]. Population dynamics of individual species are thought to be dominated by low-frequency fluctuations, that is, to display reddened fluctuations[10]. Here I report, however, that in eight nonlinear, iterative, deterministic, autonomous, discrete-time population models, some of which have been used to model real biological populations, the power spectral densities of chaotic trajectories are neither white nor reddened but are notably blue, with increasing power at higher frequencies.

The simplest discrete-time population model capable of representing the influence of environmental variability assumes that $P_{t+1}=r_tP_t$, $P_0>0$ (ref. 11). Here P_t denotes the population size (assumed to vary continuously) at time t, and r_t is a positive-valued random variable that describes the effect of environmental variation on survival and reproduction from time t to time $t+1$. In this idealized model, the population transforms a white-noise environmental input to a random-walk population trajectory, which has a reddened spectrum. To see this, suppose that r_t is identically and independently distributed for all t; r_t is thus a discrete-time white noise. Its spectrum is flat, as is shown approximately in the numerical simulations in Fig. 1*a*. The logarithm of population size $\log(P_t)=\log(P_0)+\sum_{t=0}^{t-1}\log(r_t)$ is a random walk or a discrete-time brownian motion (sometimes called brown noise), which is known to be highly reddened. The spectrum of a discrete-time random walk is illustrated in the numerical simulations in Fig. 1*b*. It would hardly be surprising if, in more realistic models or in reality, white or reddened environmental variability resulted in still redder population fluctuations.

I examined the spectra of chaotic trajectories in eight deterministic, autonomous, nonlinear population models (Table 1). In these models, P_t uniquely determines P_{t+1}, hence population fluctuations are generated by internal dynamics rather than by environmental variability. The first six models are well known and have been widely used for non-human biological populations with discrete generations[12,13]. The last two models[14,15], developed to describe human populations, have not previously been shown to behave chaotically for some parameter values. It appears not to have been noticed previously that chaotic behaviour in all eight of these models has a blue spectrum for many parameter values.

For each model, I generated 100 sample paths of 1,024 time steps, starting from an initial population size P_0 which was randomly and uniformly distributed between 0 and 1. (The Austin–Brewer model[14] was exceptional in that P_0 was uniformly distributed between 0 and 20.) I then truncated P_0 through P_{512} to eliminate any transient effects of initial conditions and checked that no population sizes were zero or negative. The remaining sequence of 512 population sizes was then tested against a sufficient condition for the existence of chaos[16]. For the parameter values shown in Table 1, all simulations satisfied the sufficient condition and were therefore shown to be chaotic. Next I calculated the fast Fourier transform (FFT) of the 512 population sizes, using the FFT function provided by Matlab version 3.5g. Because of the mirror symmetry in the spectrum with respect to its middle, I retained only the first 256 elements returned by the FFT function, dropped the first of these because it was artefactually distorted by the finite length of the time series, and multiplied each of the remaining 255 complex numbers by its complex conjugate to obtain the squared amplitude or power of the spectrum at the corresponding frequency. At each of the 255 frequencies, I computed the minimum, the maxi-

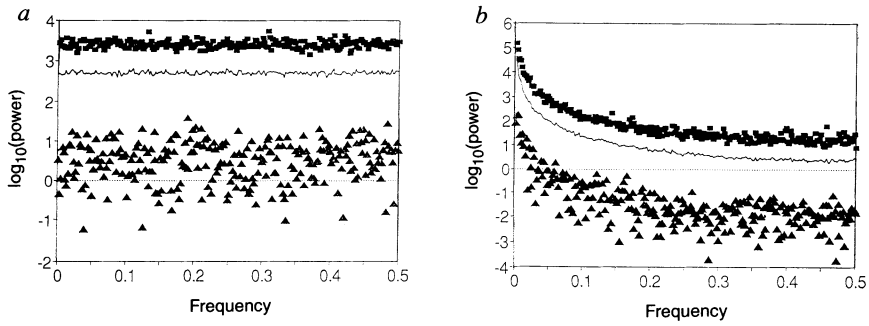

FIG. 1 Power spectral densities (spectra) of discrete-time random sequences: *a*, white noise $X_t = \varepsilon_t$, and *b*, red noise (or random walk or brown noise) $X_{t+1} = X_t + \varepsilon_t$. In both cases, ε_t is a sequence of independent and identically distributed normal random variates with mean 0 and variance 1. Sequences of length 512 were generated starting from $X_0 = 0$ and standardized to have overall mean 0 and variance 1. The fast Fourier transform and spectrum were then computed as described in the text. The continuous lines represent the average spectrum from 100 simulations; the rectangles represent the maximum spectrum; and the triangles represent the minimum spectrum. The horizontal coordinate *x* is frequency; the corresponding period is $1/x$. For example, the abscissa 0.4 corresponds to 0.4 cycles per time unit or a period of $1/0.4 = 2.5$ time units.

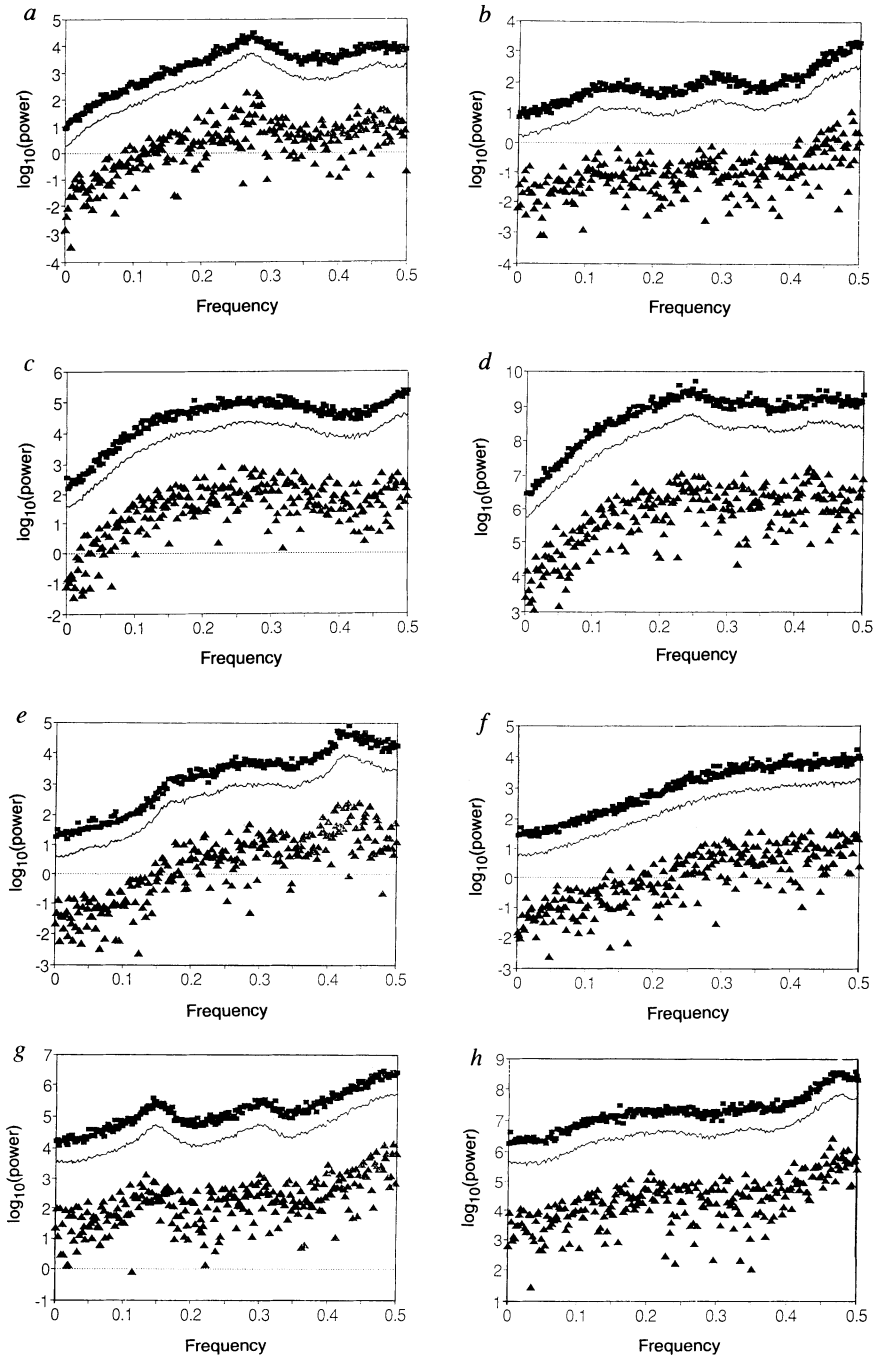

FIG. 2 Power spectral densities of eight discrete-time nonlinear population models: *a*, Moran-Ricker[12,25,26]; *b*, Verhulst[12]; *c*, Pennycuick[12,27]; *d*, Hassell[12,28]; *e*, Maynard Smith[12,29]; *f*, Varley[12,30]; *g*, Austin–Brewer[14]; and *h*, Malthus–Condorcet–Mill[15]. Table 1 gives the equations and parameter values. Symbols and units are as in Fig. 1. By contrast with the white or reddened spectra commonly observed in environmental and ecological time series, these spectra are blue, with greater power at higher frequencies.

TABLE 1 Eight nonlinear population models, with parameter values that give chaotic behaviour

Model	Parameter values*	Model name
$P_{t+1}=P_t \exp[r(1-P_t)]$	$r=3.7$	Moran–Ricker[12,25,26]
$P_{t+1}=P_t[1+r(1-P_t)]$	$r=2.7$	Verhulst[12]
$P_{t+1}=rP_t/\{1+\exp[-a(1-P_t/b)]\}$	$r=50$, $a=0.1$, $b=0.1$	Pennycuick[12,27]
$P_{t+1}=rP_t/(1+aP_t)^b$	$r=55$, $a=0.0001$, $b=100$	Hassell[12,28]
$P_{t+1}=rP_t/[1+(aP_t)^b]$	$r=5$, $a=0.5$, $b=4$	Maynard Smith[12,29]
$P_{t+1}=rP_t$ if $P_t\leqslant C$, $P_{t+1}=rP_t^{1-b}$ if $P_t>C$	$r=4$, $b=3$, $C=1$	Varley[12,30]
$P_{t+1}=P_t\{1+r[1-\exp(-sP_t)](K-P_t)\}$	$r=0.06$, $s=0.13$, $K=45$	Austin–Brewer[14]
$P_{t+1}=P_tr[K+L\log(P_t)-P_t]$	$r=0.006$, $K=600$, $L=4$	Malthus–Condorcet–Mill[15]

* Initial conditions are taken uniformly from 0 to 1, except for the Austin–Brewer model, where they are uniform between 0 and 20.

mum and the average over all 100 simulations for each model. Because the power varied widely across frequencies, the $\log_{10}$ of the power is displayed as a function of frequency in Fig. 2.

For each model, the power of fluctuations at high frequencies was at least two orders of magnitude higher, on average, than the power at low frequencies. The maximum power at the lowest frequencies often fell below the minimum power at the highest frequencies. This observation provides assurance that the apparent increase is not due to statistical fluctuations in the spectrum. Although the detailed shape of the average spectrum varied from model to model, and was not always strictly monotonically increasing, all displayed an upward trend in power with increasing frequency. Had a logarithmic scale been used for frequency, as is sometimes the case, the increase in power with increasing frequency would have been still more visually obvious. The greater apparent scatter in the minimum values compared to the maximum values results from the logarithmic transformation of the power.

These results are limited in several respects. A blue spectrum is demonstrated here only for a single point in the parameter space of each model. For most of the models, the parameter values shown are the first values tried that produced chaotic trajectories, suggesting that, within the region of parameter space that produces chaos, many points yield blue spectra. Exploratory numerical calculations suggest that the spectra of chaotic trajectories of these models are blue for many parameter values. However, in the Verhulst model, for example, for a few parameter values the spectrum has a single isolated peak (corresponding to period-3 oscillations) superimposed on a generally blue background (V. Jansen, personal communication), whereas for other parameter values the spectrum is nearly white (G. Sugihara, personal communication). In chaotic trajectories from models other than those considered here, the spectrum may similarly display isolated spikes, depending on parameter values[17]. These results do not cover all nonlinear, iterative, autonomous, deterministic discrete-generation population models that have been or could be considered. However, no models in this class that have been tested so far have had chaotic trajectories with a reddened spectrum, and, for most parameter values, chaotic trajectories that lack discrete peaks are distinctly blue. An analytical understanding of why this is so remains for the future.

The results presented here create a tension between the claims that reddened time series of natural and experimental population sizes are common or ubiquitous, and that chaotic trajectories of nonlinear population (those analysed here and similar) models are accurate descriptions of these time series[18,19]. It is not yet known whether this dilemma can be resolved by expanding the models to take account of environmental fluctuations, the interactions of single species with other species[20], or the age structure[21,22] and spatial distribution[23] of populations. Periodic and stochastic fluctuations in the parameter r of the first two models in Table 1 have already been shown to induce complex and counter-intuitive changes in the dynamics of these models[24], but the spectral effects of such fluctuations in these and additional models have not been investigated. □

Received 14 August; accepted 27 September 1995.

1. Monin, A. S., Kamenkovich, V. M. & Kort, V. G. *Variability of the Oceans* (Wiley, New York, 1977).
2. Jenkins, G. M. & Watts, D. G. *Spectral Analysis and its Applications* (Wiley, New York, 1968).
3. Steele, J. H. *Nature* **313,** 355–358 (1985).
4. Steele, J. H. *J. theor. Biol.* **153,** 425–436 (1991).
5. Steele, J. H. & Henderson, E. W. *Science* **224,** 985–987 (1984).
6. Steele, J. H. & Henderson, E. W. *Phil. Trans. R. Soc. Lond.* B **343,** 5–9 (1994).
7. Pimm, S. L. & Redfearn, A. *Nature* **334,** 613–614 (1988).
8. Arino, A. & Pimm, S. L. *Evol. Ecol.* **9,** 429–443 (1995).
9. Caswell, H. & Cohen, J. E. *J. theor. Biol.* **176,** 301–316 (1995).
10. Halley, J. M. *Trends Ecol. Evol.* (in the press).
11. Lewontin, R. C. & Cohen, D. *Proc. natn. Acad. Sci. U.S.A.* **62,** 1056–1060 (1969).
12. May, R. M. & Oster, G. *Am. Nat.* **110,** 573–599 (1976).
13. Hassell, M. P., Lawton, J. H. & May, R. M. *J. Anim. Ecol.* **45,** 471–486 (1976).
14. Austin, A. L. & Brewer, J. W. *Technol. Forecast. soc. Change* **3,** 23–49 (1971).
15. Cohen, J. E. *Science* **269,** 341–348 (1995).
16. Li, T.-Y., Misiurewicz, M., Pianigiani, G. & Yorke, J. A. *Phys. Lett. A* **87,** 271–273 (1982).
17. Farmer, D., Crutchfield, J., Froehling, H., Packard, N. & Shaw, R. *Ann. N.Y. Acad. Sci.* **357,** 453–472 (1980).
18. Schaffer, W. M. in *Chaos in Biological Systems* (eds Degn, H., Holden, A. V. & Olsen, L. F.) 233–248 (NATO Advanced Science Institutes Series A, vol. 138) (Plenum, New York, 1987).
19. Hastings, A., Hom, C. L., Ellner, S., Turchin, P. & Godfray, H. C. J. *A. Rev. Ecol. Syst.* **24,** 1–33 (1993).
20. Muratori, S. & Rinaldi, S. *SIAM J. appl. Math.* **52,** 1688–1706 (1992).
21. Levin, S. A. & Goodyear, C. P. *J. math. Biol.* **9,** 245–274 (1980).
22. Gurney, W. S. C., Nisbet, R. M. & Lawton, J. H. *J. Anim. Ecol.* **52,** 479–495 (1983).
23. Ruxton, G. D., Bascompte, J. & Solé, R. V. *J. Anim. Ecol.* **63,** 1002–1003 (1994).
24. Markus, M., Hess, B., Rössler, J. & Kiwi, M. in *Chaos in Biological Systems* (eds Degn, H., Holden, A. V. & Olsen, L. F.) 267–277 (NATO Advanced Science Institutes Series A, vol. 138) (Plenum, New York, 1987).
25. Moran, P. A. P. *Biometrics* **6,** 250–258 (1950).
26. Ricker, W. E. *J. Fish. Res. Bd Can.* **11,** 559–623 (1954).
27. Pennycuick, C. J., Compton, R. M. & Beckingham, L. *J. theor. Biol.* **18,** 316–329 (1968).
28. Hassell, M. P. *J. Anim. Ecol.* **44,** 283–296 (1974).
29. Maynard Smith, J. *Models in Ecology* (Cambridge Univ. Press, 1974).
30. Varley, G. C., Gradwell, G. R. & Hassell, M. P. *Insect Population Ecology* (Blackwell, Oxford, 1973).

ACKNOWLEDGEMENTS. I thank A. E. Cohen, J. M. Halley, V. A. Jansen, J. H. Lawton, R. M. May, G. Sugihara and an anonymous referee for help during this work, and W. T. Golden and S. L. Golden for hospitality. This work was supported by the U.S. National Science Foundation and the NERC Centre for Population Biology, Imperial College.

Visually evoked calcium action potentials in cat striate cortex

Judith A. Hirsch, José-Manuel Alonso & R. Clay Reid

The Rockefeller University, Laboratory of Neurobiology, 1230 York Avenue, New York, New York 10021, USA

EARLY intracellular studies of cerebral cortical neurons indicated that synaptic input evokes dendritic action potentials that convey information towards the soma[1]. Subsequent work *in vitro* established that neocortical neurons produce dendritic Ca^{2+} action potentials[2–5]. To determine whether natural stimuli elicit Ca^{2+} spikes, we combined the techniques of whole-cell recording[6,7], pharmacology[8] and quantitative receptive field mapping[9]. Our findings show that visual stimulation routinely evoked Ca^{2+} spikes in distinct functional[10] and anatomical[11] classes of cells in different layers of the cat striate cortex[12]. Hence regenerative Ca^{2+} potentials appear to play a role in both the initial and later stages of cortical sensory processing.